Influence of Disorder and State Filling on Charge-Transfer-State Absorption and Emission Spectra

Saeed-Uz-Zaman Khan and Barry P. Rand

Phys. Rev. Applied **16**, 044026 — Published 15 October 2021

DOI: 10.1103/PhysRevApplied.16.044026

Influence of Disorder and State Filling on Charge Transfer State Absorption and Emission Spectra

Saeed-Uz-Zaman Khan[1], and Barry P. Rand[1,2]

[1]Department of Electrical Engineering, Princeton University, Princeton, NJ, 08544, United States
[2]Andlinger Center for Energy and the Environment, Princeton University, Princeton, New Jersey 08544, USA

Abstract

We conduct comprehensive temperature dependent measurements of the charge transfer (CT) state photocurrent and emission spectra for two organic small molecule donor:fullerene (C_{60}) acceptor bulk heterojunction solar cells. We reveal that the CT spectral width and position are affected by static energetic disorder in the blend, especially evident at low temperatures. The relative contributions of the static and dynamic disorder broadening in the CT spectra are effectively extracted through consideration of a Gaussian CT energetic distribution. However, electroluminescence (EL) spectra can only be interpreted when injected carriers reach thermal equilibrium sites within the disordered density of states and emission occurs from the lowest possible CT energy. For the blend with the smaller energetic disorder, this is the case near room temperature; for the other blend with larger static disorder, carriers fail to reach thermal equilibrium sites even at room temperature and EL spectra need to be interpreted with care. For example, in the latter case, the effect of energetic disorder might not be apparent from EL spectra because the lowest energy sites are not participating. Nonetheless, these states contribute to the photocurrent generation-recombination and energy loss processes and thus demand accurate characterization, which we show is feasible through temperature dependent external quantum efficiency measurements.

1. Introduction

With the power conversion efficiency (PCE) of single-junction organic photovoltaic cells (OPVs) close to 18% [1,2], these systems are approaching their thermodynamic efficiency limit, estimated to be approximately 22-27% [3]. In order to bridge this PCE deficit, there is a need for a more comprehensive understanding of certain fundamental device processes, such as carrier generation-recombination-transport and their interplay with the physical properties of the constituent materials and processing conditions. Contrary to their inorganic counterparts, for which most electronic processes and underlying device physics are well understood, some aspects of OPVs remain elusive with unresolved questions associated with fundamental photophysical processes. A key reason behind this is the lack of understanding of intermolecular charge transfer (CT) states.

It is already established that CT state energy sets the limit for the open-circuit voltage (V_{OC}) of an OPV [4,5], governs energy losses [5–7], and plays a crucial role in charge generation and recombination processes [8–11]. However, not much is known about their energetic distribution. For example, there is not yet consensus regarding the CT density of states (DOS), with various works suggesting Gaussian [10,12,13], exponential [14,15], or some other distribution [16,17]. Due to the inherent disordered and often heterogeneous nature of organic semiconductor blends, a significant broadening of the DOS is expected and believed to play a significant role in dissociation [18–20], recombination [20–22], and transport [23–26] of charge carriers. The most important performance metrics of an OPV, energy loss [10] and V_{OC} [5,27], are directly related to the spectral distribution of the CT profile. Despite its clear influence on OPV performance, how energetic disorder, either static or dynamic, affects the CT state spectra, is still unclear. Some research supports that CT emission spectra are strongly affected by disorder [10,12,16], while others suggest the opposite [5,13,28]. For example, it has been shown that a simple convolution of CT electron-hole DOS is insufficient [13,14] to approximate the spectra, due to the incomplete relaxation of the optically excited or electrically injected carriers within the disordered DOS, respectively for photoluminescence (PL) [29] or electroluminescence (EL) [13,14]. Thus, emission spectra need to be treated with caution as EL will not originate from the lowest possible energetic states in an OPV if excited carriers do not reach thermal equilibrium before recombining. Since absorption and emission spectra allow probing the disordered DOS and are crucial for experimental characterization of the CT state energy [4,5,30,31], understanding the effect of disorder on the CT state spectra and how it responds to various physical conditions, like temperature and the degree of carrier injection, are of significant importance.

The spectra of CT states are often described [5] in the framework of the Marcus theory of electron transfer [32], where the absorption and emission spectra mirror each other and their intersection point defines the CT state energy. The expression defining the emission spectrum is derived assuming reciprocity between light emission and photocurrent [5,33] and assumes that carriers are under thermal equilibrium. In this framework, the external quantum efficiency (EQE) and the reduced emission spectra from CT states are respectively given as [5]

$$\eta_{EQE}(E) = \frac{f}{E\sqrt{4\pi\lambda k_B T}}\, exp\left(\frac{-(E_{CT}+\lambda-E)^2}{4\lambda k_B T}\right) \qquad \text{(Eq. 1)}$$

$$\frac{I_{EL}(E)}{E} = \frac{f_{EL}}{\sqrt{4\pi\lambda k_B T}}\, exp\left(\frac{-(E_{CT}-\lambda-E)^2}{4\lambda k_B T}\right) \qquad \text{(Eq. 2)}$$

where E_{CT} and λ are the CT state and reorganization energy of the electron transfer process, respectively. The factor f is proportional to the donor-acceptor (D-A) electronic coupling, k_B is Boltzmann's constant, T is temperature, and q is the elementary charge. The value of λ defines the absorption and emission spectral broadening in the classical Marcus picture, and has been shown to be related to thermally activated intramolecular and intermolecular low-frequency

vibrations [12,28,34]. As apparent from Eq. 1-2, the energy difference between the peaks of absorption and emission spectra (i.e. Stokes shift) is 2λ. This description of the CT spectra ignores any contribution from static disorder and assumes only dynamic (vibrational) spectral broadening. Additionally, this framework predicts vanishingly small spectral linewidth as temperature goes down towards zero Kelvin, an aspect that is not observed experimentally [12,28]. The Stokes shift also deviates from 2λ, and E_{CT} extracted from temperature dependent EQE spectra shows a seemingly unphysical roll-off with decreasing temperature, both of which have been attributed to the existence of energetic disorder [5], which is not explicitly considered in Eq. 1-2. Nonetheless, this method has been successfully utilized to fit CT spectra [5,9,29,35–39] and often performs quite well near room temperature.

Burke et al. proposed a modification [10] to the previously described formalism (Eq. 1-2) by considering a Gaussian energetic distribution of CT states. They demonstrated that when a Gaussian CT DOS is considered, the resultant absorption spectra would remain Gaussian, following the expression

$$\eta_{EQE}(E) \propto \frac{1}{E\sqrt{2\pi(\sigma_{CT}^2+2\lambda k_B T)}} exp\left(\frac{-(E_{CT}+\lambda-E)^2}{2\sigma_{CT}^2+4\lambda k_B T}\right) \qquad \text{(Eq. 3)}$$

Whereas, the reduced emission spectrum, introduced by Linderl et al. [16] following reciprocity approximation, is expressed as

$$\frac{I_{EL}(E)}{E} \propto \frac{1}{\sqrt{2\pi(\sigma_{CT}^2+2\lambda k_B T)}} exp\left(\frac{-\left(E_{CT}-\lambda-\frac{\sigma_{CT}^2}{k_B T}-E\right)^2}{2\sigma_{CT}^2+4\lambda k_B T}\right) \qquad \text{(Eq. 4)}$$

which should only be applicable if all the conditions for reciprocity (quasi-thermal equilibrium population of the CT excitons within the DOS, for example) are fulfilled. When experimental EQE data are fit with the classical Marcus-type expressions (Eq. 1-2), one extracts an effective CT energy, $E_{CT(exp.)}$ and reorganization energy, $\lambda_{(exp.)}$. The peak of the Gaussian DOS distribution (E_{CT}) and true reorganization energy (λ) are connected to the experimentally extracted values through the following expressions:

$$E_{CT(exp.)} = E_{CT} - \frac{\sigma_{CT}^2}{2k_B T} \qquad \text{(Eq. 5)}$$

$$\lambda_{(exp.)} = \lambda + \frac{\sigma_{CT}^2}{2k_B T} \qquad \text{(Eq. 6)}$$

Here, σ_{CT} is the average standard deviation of the lowest energy CT state DOS in the bulk. From Eq. 5 it is evident that the experimentally evaluated peak CT state energy from the EQE spectra will be temperature dependent if the CT energetic spread (σ_{CT}) is sufficient ($> k_B T$ at room temperature), which indeed it is in many OPV blends. [5,10] With the aid of temperature dependent EQE and Eq. 5 and 6, one could also extract σ_{CT} and thus the effective CT Gaussian DOS.

The energetic disorder in the CT state should be a result of the static disorder in both the donor and the acceptor, since both constitute the CT state. In a simplified picture, assuming electrons and holes reach thermal equilibrium, the CT EL should correlate to the joint density of states (JDOS) obtained from convoluting the donor-HOMO (hole) and acceptor-LUMO (electron) DOS [13]. In the case of a Gaussian energetic distribution of donor-HOMO with a standard deviation σ_D and acceptor-LUMO with a standard deviation σ_A, the JDOS convolution results in a CT standard deviation of $\sqrt{\sigma_A^2 + \sigma_D^2}$. So, even in the case of low acceptor disorder in an acceptor rich blend, the overall CT disorder could be high.

In Burke et al.'s work on a disordered polymer:fullerene blend, the extracted CT state static disorder (σ_{CT}) was found to be ~104 meV [10], which is twice that of its dynamic counterpart at 300 K [28], thus highlighting the significance of incorporating CT energetic disorder when interpreting the spectra. Kahle et al. [12] reached a similar conclusion in the study of a different polymer:fullerene system, where PL data did not show significant spectral narrowing down to 5 K, contrary to expectations from the Marcus-type expressions (Eq. 1 and 2). Also notable, they only observed a very small blue shift of the emission peak with reductions in temperature whereas Burke et al.'s work predicts a redshift. The authors reported no change in the shape of the CT photocurrent spectra as temperature reduced from 295 to 50 K.

It has been suggested [14] that disorder-induced localized exponential tail states are not represented in the emission spectra, as they are suppressed due to the large spatial separation between electrons and holes at these energies. Rather, more delocalized higher energy states partake in the emission process, which is justified from the absence of the shift in emission peak with increasing bias expected from the exponential DOS filling [14]. This is an indication that carriers that are radiatively recombining are not in the lowest possible energy states i.e. not in thermal equilibrium. However, this bias insensitivity of the emission peak could also be a result of a Gaussian (rather than exponential) CT DOS. [13]

The interpretation of the CT state emission spectra are further complicated due to the possibility of non-thermal occupation of the DOS, as demonstrated initially by Brigeman et al [40]. By the term "non-thermal equilibrium" occupation, it is implied that the CT excitons are not in quasi-thermal equilibrium within the CT DOS manifold. Studying subphthalocyanine:C_{60}, it was found that the steady state PL peak blue shifts as temperature was reduced. This blue shift is evidence of an inability to reach the lowest possible energy sites before recombination. This incomplete thermalization is expected to become extreme with increasing disorder in the blend. This may also explain the common observation of redshifted EL compared to PL [40,41]. For EL, injected carriers are likely to fill the DOS from the bottom up and should reflect a carrier population closer to thermal equilibrium. Concomitantly, this casts doubt on the reliability of PL to extract spectral information of the CT state [40,42], especially in the case of a blend with a high degree of disorder. Additionally, Melianas et al. [13] found states ~180-570 meV below the

experimentally observed CT-EL peak, i.e. EL emission also could occur from higher energy states rather than the completely relaxed one within the DOS, and this gap diminishes at lower disorder. Although hidden from emission spectra, these non-emissive states can potentially take part in photon absorption, charge generation-recombination, and transport, when operated as a solar cell. Recently, temperature dependent EL and PL measurements on several bulk heterojunctions (BHJs) demonstrated that spectral linewidth narrows linearly and then tends to saturate below a certain material dependent temperature [28]. The linewidth saturation was explained by a Franck-Condon formalism accounting for both high and low frequency vibrational modes, without having to invoke static disorder. In addition, authors noted a redshift of the EL peak as temperature goes down, as expected from Eq. 3-6.

In this work, we provide additional insight to address some of the apparent aforementioned discrepancies regarding the relative influence of static and dynamic disorder in the CT state spectra. We study two archetypal small molecule BHJ OPVs, TAPC:C_{60} and NPB:C_{60} (TAPC is 1,1-bis[(di-4-tolylamino)phenyl]cyclohexane and NPB is *N,N′*-di(1-naphthyl)-*N,N′*-diphenyl-(1,1′-biphenyl)-4,4′-diamine), that have different CT energetic disorders. Through temperature dependent EQE and EL measurements, we find that the spectral linewidth narrows linearly and leads to a non-zero value when extrapolated to zero Kelvin. For NPB:C_{60}, the blend with larger energetic disorder, the zero Kelvin linewidth yields a value larger than that of TAPC:C_{60}. From emission, TAPC devices show a larger red shift of the EL peak compared to the NPB devices in the same decreasing temperature range. For NPB devices, we find the CT EL peaks are much higher in energy than what is expected from reciprocity, whereas for TAPC devices, the EL peaks could be predicted from reciprocity down to a certain temperature. We rule out any effect of elevated substrate temperature, due to Joule heating, as a reason for this discrepancy. Rather, we assert that this is a direct consequence of energetic disorder that prevents complete thermalization of the injected carriers within the disordered DOS and emission occurs from higher energy. From the shift in the emission peak position with increasing current, we confirm a Gaussian DOS filling and fully rationalize this choice of DOS function. We also emphasize that caution must be taken when using emission spectra, either PL or EL, as injected carriers might not reach complete thermal equilibrium. In those cases, fitting the experimental emission spectra using Eq. 2 or 4 would result in inaccurate values of E_{CT} and spectral linewidth. Overall, we demonstrate that static disorder indeed affects CT spectral properties to an extent that depends on the magnitudes of static disorder and temperature.

2. Methods

Solar cell preparation: Small molecular organic materials bathocuproine (BCP) (Lumtec), NPB (Nichem), TAPC (Lumtec), and C_{60} (Nano-C) were purchased from commercial vendors and further purified using vacuum thermal gradient sublimation method. Molecular structures,

ionization energies and electron affinities of the materials [43,44] are provided in Table S1 of the Supplemental Material [45].

Solar cells were grown on pre-patterned ITO-glass substrates purchased from Colorado Concept Coatings. The substrate cleaning process started with sonication in soapy water, followed by deionized water for 15 min at 40 °C. Then the process is repeated with acetone and isopropanol at 40 °C for 10 min. Finally, the substrates were treated with O_2 plasma for 10 min.

Both TAPC:C_{60} and NPB:C_{60} devices were fabricated through vacuum (~10^{-7} Torr base pressure) thermal co-evaporation of the donor-acceptor on top of the cleaned substrates. The structure of the devices was ITO/donor:C_{60} (50 nm)/BCP (10 nm)/Al (100 nm). The active area of each device is 0.1 cm^2.

EQE Characterization with temperature variation*:* The EQE measurements were performed using a Newport TLS-300X tunable light source. The monochromatic light beam output from the source was passed through an optical chopper with the frequency set at 390 Hz. The devices were kept at short circuit condition and the output photo-current was taken to a current-to-voltage pre-amplifier (SR570, Stanford Research Systems). The voltage output of the preamplifier was taken to a Stanford Research Systems SR830 lock-in-amplifier which demodulated the photocurrent contribution of the monochromatic light. To estimate the number of incident photons in the light, calibrated Si and Ge photodiodes from Newport were used.

To control substrate temperature, the devices were kept inside a Janis VNF-100 Cryostat. Temperature setpoints were controlled and monitored using a cryogenic temperature controller (LakeShore 335). The devices were first cooled down to 80 K using liquid N_2 vapor inside the cryostat and then gradually heated up to each temperature setpoint for taking the measurement. Room temperature EQE spectra before and after cool down did not show any signs of device degradation.

Electroluminescence measurement with temperature variation: EL was collected from the devices using SpectraPro HRS-300 spectrometer coupled with a PIX-400B CCD camera from Princeton Instruments. Constant current to the devices was supplied from a Keithley 2400 source meter. The devices were kept inside the cryostat described in the EQE measurement section. The light output from the devices were taken to the spectrometer using a fiber optic cable. The spectrometer was wavelength corrected using the IntelliCal calibration system from Princeton Instruments. The intensity of the spectrometer was corrected using a HL-3P-CAL calibration lamp source from Ocean Insight. Background correction was applied to the data set during the measurements. Inside the cryostat, a rough pump continuously forces N_2 vapor flow over the sample. Since the sample sits in flowing N_2 vapor, it reaches thermal equilibrium with the vapor swiftly and prevents sample heating. The large metal cathode (0.1 cm^2 device area) of the device, exposed to the flowing N_2 vapor should be able to transfer any heat generated in the device promptly. As an added precaution, to reduce the effect of resistive heating and device degradation due to prolonged current flow, the current source was only turned on for a brief period (10-20 s), at the moment the spectrum was captured. In between each injection current change, there was a 5-10 min rest period.

3. Results and Discussion

The donor-acceptor blends TAPC:C_{60} and NPB:C_{60} are deposited at 1:16 volume ratio through thermal evaporation. Details of the materials and device fabrication can be found in the methods section. External quantum efficiency measurement and subsequent fitting of the sub-gap EQE tail with a Gaussian function (Eq. 3-6) reveal the room temperature $E_{CT(\text{exp.})}$ to be 1.45 eV and 1.39 eV, respectively for TAPC:C_{60} and NPB:C_{60} (see Fig. S1(j) and S2(h) in the Supplemental Material for the fitting details [45]). The reorganization energies $\lambda_{(\text{exp.})}$ of the two devices were slightly different, 0.13 eV and 0.21 eV for TAPC:C_{60} and NPB:C_{60}, respectively. Since, $\lambda_{(\text{exp.})}$ embodies the vibrational (homogenous) broadening of the absorption/emission spectra according to the Marcus description of the CT state energy, the absorption/emission linewidth of these devices are also expected to be in accordance with their respective $\lambda_{(\text{exp.})}$, at least in the temperature range where vibrational broadening dominates.

Photocurrent Spectra at Various Temperatures:

From an EQE spectrum, it is possible to approximate the CT state absorption spectrum using Eq. 1-4. However, from the room temperature spectrum it is not possible to estimate the relative contributions of static and dynamic broadening [13,16]. Therefore, we performed temperature dependent EQE measurements on both the TAPC:C_{60} and NPB:C_{60} blends. Figure 1(a) shows the temperature dependent EQE of a TAPC:C_{60} solar cell. With decreasing temperature, the EQE steadily decreases owing to the inferior charge transport and dissociation efficiency [46] at low temperatures. The CT EQE tails normalized at 1.57 eV are shown in the inset, and demonstrate narrowing of the spectra with decreasing temperature. Detailed normalized CT EQE spectra are provided in Fig. S3(a) of the Supplemental Material [45]. Figure 1(b) shows the percent change in EQE, revealing the effect of the temperature change at different excitation energies. The second derivative-like lineshape centered at ~1.6 eV is indicative of a red shift of the CT absorption spectra (low energy EQE tail) with reducing temperature, an effect that has been reported before for other OPVs [5,34]. The temperature dependent shift in E_{CT} is clear when the EQE tail is fitted with a Gaussian function following Eq. 3 (each fit shown in Fig. S1(a-j) of the Supplemental Material [45]). Figure 1(c) shows the extracted $E_{CT(\text{exp.})}$, displaying a clear roll off with decreasing temperature. At the same time, $\lambda_{(\text{exp.})}$ increases as temperature drops. The peak of the CT absorption spectrum, designated by $E_{CT(\text{exp.})} + \lambda_{(\text{exp.})}$, also slightly red shifts with decreasing temperature as displayed in Fig. 1(d). The full width at half maximum (FWHM) of the CT absorption spectrum reduces with temperature, as expected from the contribution from vibrational (Franck-Condon) broadening. Nonetheless, it does not go to zero as expected from the simple Marcus description of CT absorption in the absence of static disorder broadening (Eq. 1).

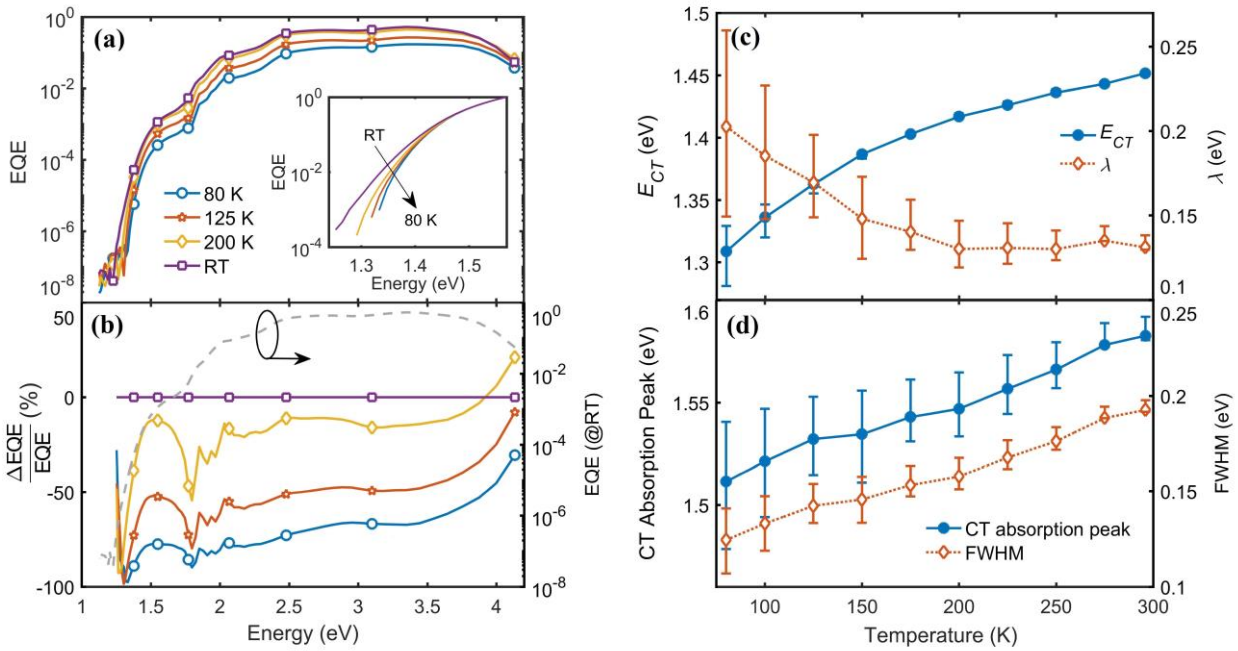

Figure 1. (a) External quantum efficiency (EQE) spectra of TAPC:C_{60} for substrate temperatures ranging from 80-296 K. The CT EQE spectral tails, normalized at 1.57 eV, are shown in the inset. (b) Percent change in EQE with respect to room temperature (296 K). (c) Extracted values of $E_{CT(\text{exp.})}$ (blue circles) and $\lambda_{(\text{exp.})}$ (red diamonds) as a function of temperature. (d) CT absorption peak (blue circles) and FWHM (red diamonds) as a function of temperature. The error bars were obtained by varying the data window in the low energy EQE tail used to fit Eq. 3.

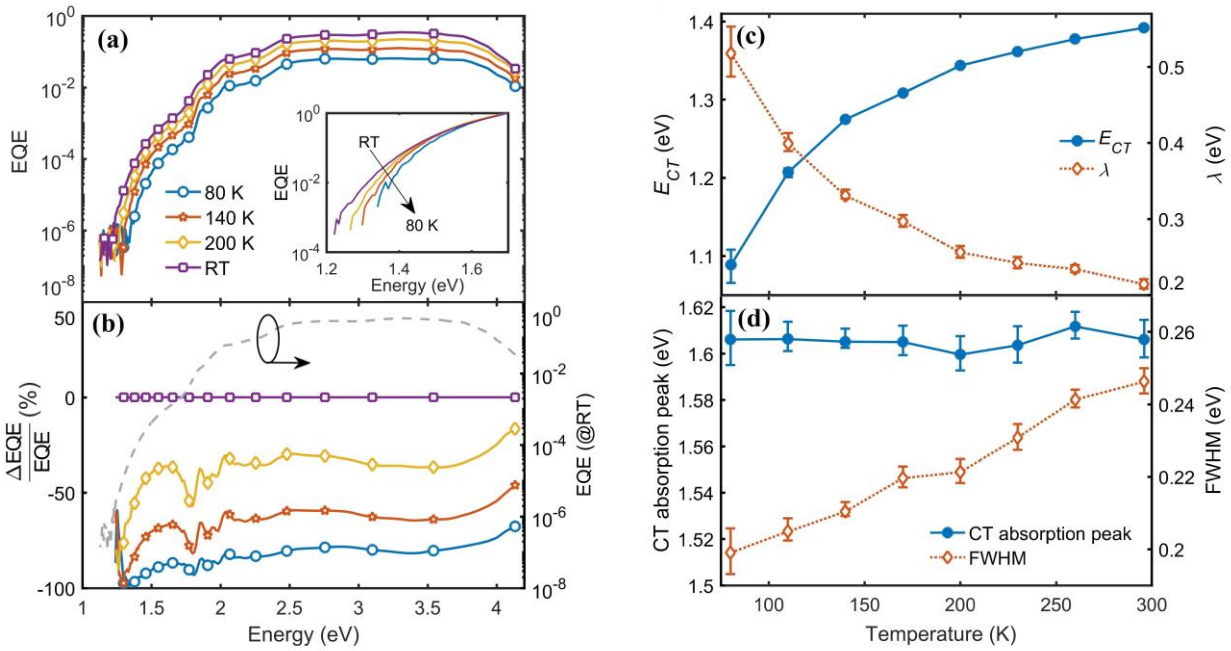

Figure 2. (a) External quantum efficiency (EQE) spectra of NPB:C_{60} for substrate temperatures ranging from 80-296 K. The CT EQE spectral tails, normalized at 1.7 eV, are shown in the inset. (b) Percent change in EQE with respect to room temperature (296 K). (c) Extracted values of $E_{CT(\text{exp.})}$ (blue circles) and $\lambda_{(\text{exp.})}$ (red diamonds) as a function of temperature. (d) CT absorption peak (blue circles) and FWHM (red diamonds) as a function of temperature. The error bars were obtained by varying the data window in the low energy EQE tail used to fit Eq. 3.

Figure 2 presents the results of temperature dependent EQE measurements of the NPB:C_{60} device. Like TAPC:C_{60}, the EQE of NPB:C_{60} is suppressed with temperature (Fig. 2(a)), and the percentage change in EQE (Fig. 2(b)) displays a similar 2nd derivative-like lineshape near the CT absorption peak, indicating a red shift of the spectral tail with decreasing temperature. The CT EQE tails normalized at 1.7 eV are shown in the inset, confirms that the shift in the EQE tail is originating from the narrowing of the spectra with decreasing temperature. Details of normalized CT EQE spectra could be found in Fig. S3(b) of the Supplemental Material [45]. The complete fitting of the temperature dependent EQE spectra (detailed in Fig. S2(a-h) of the Supplemental Material [45]) allows to track how $E_{CT(\text{exp.})}$ and $\lambda_{(\text{exp.})}$ change with temperature (Fig. 2(c)), revealing similar behavior as the TAPC:C_{60} devices. The FWHM of the CT absorption spectra also decrease with temperature (Fig. 2(d)), similar to the TAPC devices.

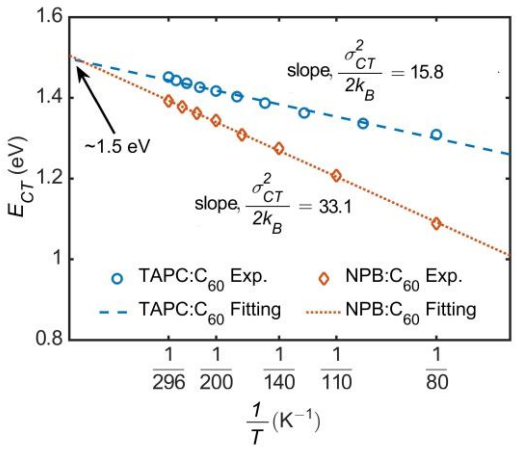

Figure 3. Extraction of the CT energetic distribution standard deviation (σ_{CT}), for TAPC:C60 (blue circles) and NPB:C60 (red diamonds) solar cells. Dashed lines show the linear fitting through the experimental data points. The y-intercepts yield E_{CT} values of 1.50 eV and 1.51 eV, respectively for the TAPC and NPB devices. The slopes of the fitted lines are equal to $\frac{\sigma_{CT}^2}{2k_B}$, yielding $\sigma_{CT} = 52 \pm 5$ meV for TAPC:C60 and $\sigma_{CT} = 76 \pm 3$ meV for NPB:C60. The uncertainties in σ_{CT} are estimated considering the error bars in E_{CT} values from Fig. 1c and 2c.

From the temperature dependent $E_{CT(\text{exp.})}$ values, it is possible to extract the standard deviation of the static CT state energetic distribution (σ_{CT}) [10]. Figure 3 shows $E_{CT(\text{exp.})}$ vs. $\frac{1}{T}$ for both devices from which σ_{CT} = 52 ± 5 and 76 ± 3 meV for TAPC:C60 and NPB:C60, respectively, following Eq. 5, while extracted E_{CT} values are 1.50 eV and 1.51 eV, respectively. The FWHM of the absorption spectra, when extrapolated to zero Kelvin, gives values of 100 and 180 meV, respectively for TAPC:C60 and NPB:C60 (Fig. S4 of the Supplemental Material [45]). When translated to standard deviation, assuming a Gaussian function, these become σ_{CT}= 43 ± 8 and 76 ± 2 meV, again NPB:C60 has a higher value, consistent with the findings from the $E_{CT(\text{exp.})}$ fitting. The uncertainties in σ_{CT} are estimated considering the error bars in E_{CT} values from Fig. 1c and 2c. We could also fit the $\lambda_{(\text{exp.})}$ values shown in Fig. 1(c) and 2(c) with Eq. 6, and extract λ = 0.10 eV for TAPC:C60 and λ = 0.11 eV for NPB:C60. Static disorder values obtained from our devices are in the same order magnitude as other BHJ blends [12,13] and approximately half of the typical values of dynamic disorder ($\sqrt{2\lambda k_B T}$) at room temperature.

Emission Spectra at Various Temperatures:

Organic solar cells are often assumed to follow absorption-emission spectral reciprocity [5]. However, as discussed in the introduction, PL spectra may not provide an accurate picture due to the non-thermal DOS site occupation [40], particularly at low temperatures. On the other hand, EL spectra appear to be a more viable indicator of the CT spectral characteristics, especially when done in constant current injection mode to ensure the same level of DOS filling across the temperature range of the measurement. The complete set of EL spectra can be found in Fig. S5(a-h) and S7(a-h) of the Supplemental Material [45], respectively for TAPC:C_{60} and NPB:C_{60}, for temperature setpoints from 80 to 296 K (RT) at 30 K intervals (EL spectra for both devices are provided in semi-log scale in Fig. S6 and S8 of the Supplemental Material [45]). As representative data, in Fig. 4, only the 80 K and RT emission spectra for both devices are shown. Note that, spectra shown in Fig. 4 are refined by applying a smoothing filter on the raw spectra obtained from the spectrometer. Figure S9 of the Supplemental Material [45] demonstrates the reliability of this smoothing operation, by comparing the raw and smoothened EL spectra of TAPC:C_{60} at RT. The normalized EL spectra at different injected current density could be found in Fig. S10 and S11 of the Supplemental Material [45], respectively corresponding to Fig. 4(a) and Fig. 4(b).

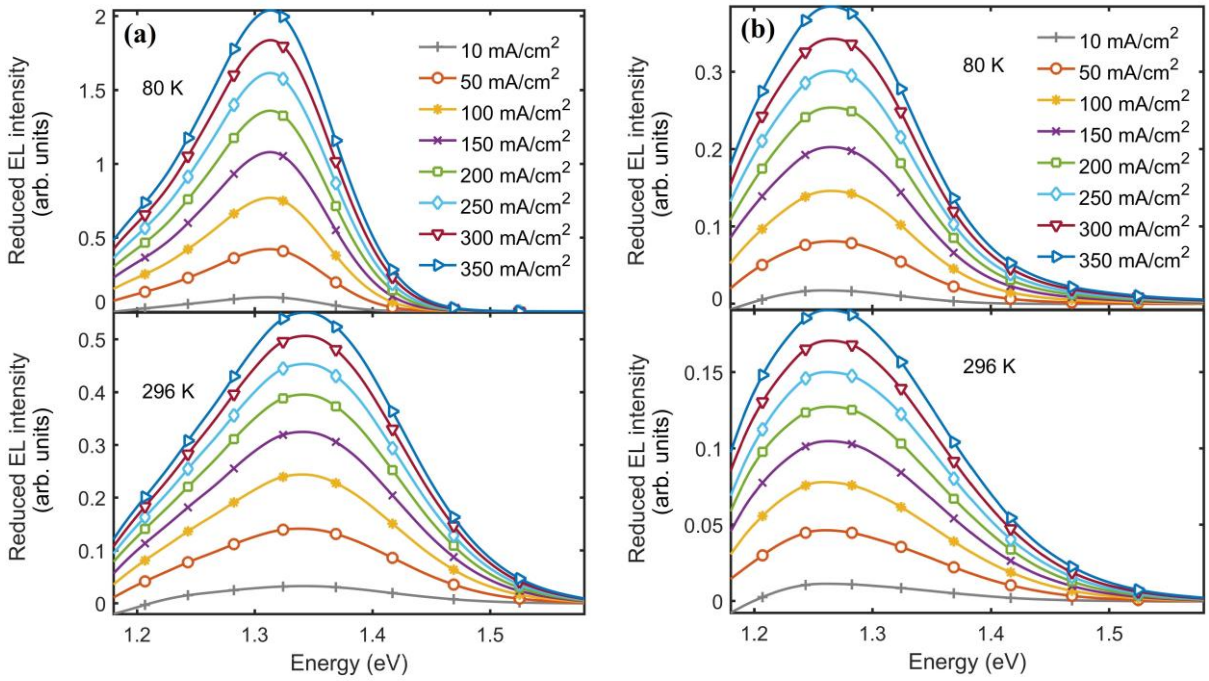

Figure 4. Reduced EL spectra for injection current densities ranging from 10-350 mA/cm^2 for (a) TAPC:C_{60} and (b) NPB:C_{60} solar cells. The top and bottom spectra are for 80 and 296 K substrate temperatures, respectively. Spectral linewidth narrows as the temperature reduces from 296 to 80

K for both devices. The TAPC:C_{60} spectral peak red shifts by ~30 meV in this temperature range, whereas the NPB:C_{60} peak remains nearly fixed.

Figure 4(a) shows the TAPC:C_{60} EL spectra at 80 K (top) and RT (bottom) with injection current densities varying from 10-350 mA/cm^2. Comparison of the spectral peaks reveal a red shift of ~30 meV (Fig. S12 of the Supplemental Material [45]) as temperature reduces from 296 to 80 K. Also, there is a small EL peak blue shift with increasing injection current density, discussed below. The spectral linewidth linearly narrows, due to the reduction in vibrational broadening at lower temperatures (Fig S13(a) of the Supplemental Material [45]). When compared to the linewidth of the TAPC:C_{60} CT absorption spectra (Fig. 1(d)), the linewidth from the EL matches quite well in the experimental temperature range. Also, the linewidth of the EL spectra without any contribution from vibrational broadening at zero kelvin (0 K linewidth) at 150 mA/cm^2 injection current density is 0.11 eV (Fig. S13(a) of the Supplemental Material [45]), which matches well with the value from the absorption spectra (Fig. S4 of the Supplemental Material [45]). The EL spectra could be fitted with a Gaussian shape for various carrier injection and temperature conditions, as shown in Fig. S14 of the Supplemental Material [45].

Figure 4(b) displays the temperature dependent EL spectra for NPB:C_{60} devices, at the same injection current density range used for TAPC:C_{60}. As can be seen from Fig. S13(b) of the Supplemental Material [45], the RT linewidth of NPB:C_{60} emission is ~0.19 eV, similar to the 80 K linewidth we get from the absorption spectra (Fig. 2(d)), meaning the complete CT DOS is not represented in the emission spectra. The EL linewidth shows a similar narrowing as TAPC:C_{60} down to 200 K, below which it saturates (Fig. S13(b) of the Supplemental Material [45]). On the other hand, the peak position remains unchanged with temperature (Fig. S12 of the Supplemental Material [45]). The lineshape of the spectra remains Gaussian with the temperature variation at different injection current densities (Fig. S15 of the Supplemental Material [45]). For both the TAPC:C_{60} and NPB:C_{60} devices, the slopes of EL peak position vs. injected current density curves are significantly smaller than ~60 meV/dec at RT (Fig. S16 of the Supplemental Material [45]), as expected from a Gaussian CT DOS filling [16].

For NPB:C_{60}, the saturated linewidth of the EL spectra (Fig S13(b) of the Supplemental Material [45]) is close to the 0 K extrapolated linewidth of the CT absorption spectra (Fig. S4 of the Supplemental Material [45]). Similar EL linewidth saturation has been reported for other OPV blends [16,28], but in our case the linear part, when extrapolated to 0 K gives a linewidth of 0.13 eV (Fig. S13(b) of the Supplemental Material [45]), a finite value, as expected from a blend with static disorder broadening according to Eq. 4. In the literature, however, the extrapolated 0 K linewidth is reported to be near zero [16] or, even negative [28]; the latter situation was explained by invoking full Franck-Condon formalism to describe the CT emission considering both high and low frequency vibrational modes, disregarding static disorder. It is worth mentioning that these studies did not include temperature dependent CT absorption spectra. In our measurement, both

absorption and emission spectra provide a finite 0 K linewidth value, which suggests that static disorder indeed influences the spectral shape, to an extent which depends on the degree of disorder in the blend.

That the absorption spectral linewidth and peak of NPB:C_{60} experience a steady decrease in value with temperature, whereas emission spectra do not follow this trend, is likely a consequence of non-thermal occupation of carriers within the CT DOS [13,40]. To rule out alternatives, we verified that the saturation of the linewidth or the emission peak is not a result of Joule heating during the EL measurements. If local heating is present, the internal cell temperature would be higher than the substrate temperature, which is in equilibrium with the cryostat, an effect that would be more severe at low temperatures, and which would alter the expected temperature dependence of the spectral peak or linewidth. During our measurements we took special care to prevent local heating, as detailed in the methods section. Analysis of the EL spectral data also supports this claim due to the following reasonings: first, the lowest and highest injection current density peak positions have the same trend with respect to the temperature change (Figure S12 of the Supplemental Material [45]); second, the spread of the FWHM for the studied injection current density range are the same at different temperatures, ~50 and 54 meV, respectively, at 80 and 296 K (Figure S13(b) of the Supplemental Material [45]) for NPB:C_{60}. If local heating were an issue, the FWHM spread at 80 K should be much larger than the spread at 296 K; and third, the absolute count of the EL spectra from the spectrometer increases monotonically with the decreasing substrate temperature for both the TAPC:C_{60} and NPB:C_{60} devices (Fig. S5(a-h) and S7(a-h) of the Supplemental Material [45]), indicating that device internal temperature is not elevated. More on this point can be found in Note I of the Supplemental Material [45].

The D-A systems considered in this study have very low donor content, which ensures optimal device performance [9]. However, considering fullerene is expected to have significantly higher mobility than the donors in such blends [47], it is worth considering whether unbalanced charge injection/transport is responsible for the deviation from reciprocity [48]. Linderl et al. [16] reported the EL of DBP:C_{60} (1:1) (where DBP is 5,10,15,20-tetraphenylbisbenz[5,6]indeno[1,2,3-cd:1′,2′,3′-lm]perylene) as a function of temperature, which demonstrates non-thermal equilibrium behavior as well (i.e. saturation of linewidth at low T and EL peak position staying relatively constant with temperature, similar to NPB:C_{60}). For the DBP:C_{60} device, a layer of PEDOT:PSS exists between ITO and the blend, which likely improves hole injection in the device. Also, DBP reportedly has a hole mobility of 3×10^{-2} cm^2/Vs [49], comparable to the electron mobility in C_{60} [50]. This suggests that low donor blend ratio or electron-hole mobility discrepancy in the blend are not the primary contributing factors behind the deviation in reciprocity.

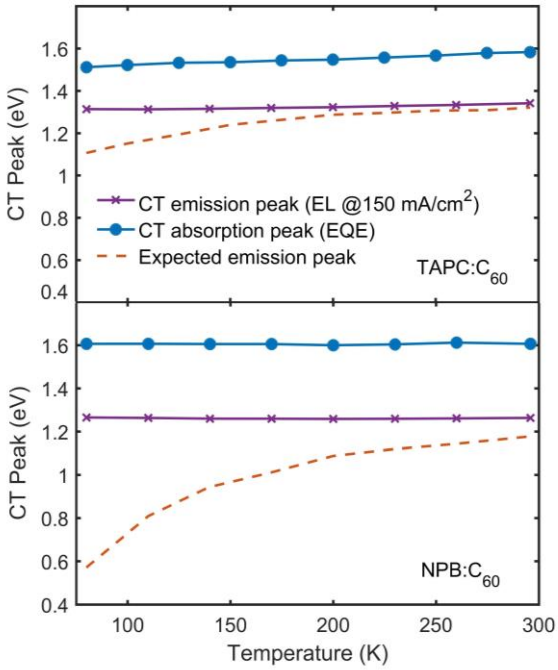

Figure 5. Approximation of the CT emission peak from the absorption peak, assuming absorption and emission spectra maintain reciprocity. The solid line with blue circles is the experimental CT absorption peak ($E_{CT(\text{exp.})} + \lambda_{(\text{exp.})}$). The solid line with purple crosses is the experimental emission (EL) peak from Fig. S12 of the Supplemental Material [45], at 150 mA/cm^2 injection current density. The red dashed line is the expected emission peak, $E_{CT(\text{exp.})} - \lambda_{(exp.)}$, estimated from the absorption peak. The $E_{CT(\text{exp.})}$ and $\lambda_{(exp.)}$ values used are shown by the blue circles and red diamonds in Fig. 1(c) and 2(c), that correspond to $\sigma_{CT} = 52 \pm 5$ meV for TAPC:C_{60} and $\sigma_{CT} = 76 \pm 3$ meV for NPB:C_{60}. The top figure is for TAPC:C_{60}, whereas the bottom one is for NPB:C_{60}.

Effect of Disorder on Spectral Shape and Position:

The CT emission peak can be approximated from the absorption peak following Eq. 3 and 4. Figure 5 plots the experimental EL peaks along with that expected from absorption for both the TAPC:C_{60} and NPB:C_{60} devices. For TAPC devices, the experimental EL peaks are very close to the expected values near room temperature, with deviation at low temperatures where experimental peaks are slightly higher in energy. On the other hand, for NPB:C_{60}, even at room temperature the experimental peak is much higher than what is expected from the absorption spectra. Since we ruled out heating, this trend in EL peak is explained through non-thermal occupation of the CT states, meaning the injected carriers are not relaxing to the lowest possible CT state within the disordered DOS. For a blend with small disorder, TAPC:C_{60} in our case, the carriers are still able to reach the lowest possible sites at temperatures above 200 K. For low temperatures however, carriers fail to thermalize and instead emit from higher energy sites. For a blend with large disorder,

NPB:C_{60} in our case, even at room temperature carriers cannot reach the lowest possible sites before recombining radiatively. During optical excitation, both the lower and higher energy sites in a disordered blend can absorb the excitation and CT EQE represents the entire CT DOS. But upon voltage bias, injected carriers might not reach their respective lowest energy sites, which might also be at separate spatial locations [13], and thus not form the lowest energy CT excitons. As a result, the low energy tail of the CT DOS will remain unfilled (i.e. CT excitons will not reach quasi-thermal equilibrium within the CT DOS) and emission will occur from a higher energy state. So, the EL spectra will only represent a higher energy subset of the CT DOS, while the absorption spectra (EQE) will represent the complete DOS. As the carrier transport pathways through the blends become more torturous with higher disorder and lower temperature [40], carriers in such conditions are less likely to reach the lowest energy sites and the discrepancy between CT DOS estimated from EL and EQE spectra will become more prominent. The non-thermal occupation of sites is not exclusive to the organic blends we discussed, but rather observed in many other blends. Brigeman et al. [40] demonstrated this for PL emission of NPB:C_{60}, subphthalocyanine:C_{60} and a poly(p-phenylene vinylene):fullerene blend. More recently, Melianas et al. [13] demonstrated that EL can suffer from non-thermal carrier distribution for several polymer-fullerene D-A blends, and reported that the gaps between experimentally observed EL peaks and lowest thermal equilibrium energy sites are indeed energetic disorder dependent and go to zero at low disorder values, which is indeed what we see from Fig. 5 at RT. However, Melianas et al. did not explore temperature dependence of the emission peak. The fact that the emission from the devices deviates further away from thermal equilibrium at lower temperatures, and we see the gap between the experimental peaks and those expected from absorption-emission reciprocity increases with reducing temperature, strengthens our arguments about disorder induced non-thermal carrier distribution influencing the emission spectral features. We would like to note that, very recently Göhler et al. [51] offered an alternative hypothesis to explain the spectral features of OPVs. By performing a global fit on the EL-EQE spectra over a range of temperatures, the authors found that electro-optical reciprocity is held as long as an elevated device temperature is assumed for the emission spectra and multiple vibrations are considered. We performed similar reciprocity analysis of the EL-EQE data presented in this work and found that for 80 K substrate temperature (which is assumed to be the device temperature during the EQE measurements), 1040 K and 1600 K device temperatures are required to fit the emission spectra, respectively for TAPC:C_{60} (Fig. S17 of the Supplemental Material [45]) and NPB:C_{60} (Fig. S18 of the Supplemental Material [45]). Although resistive heating could be a real issue in some blends, we found no evidence of that in our data (see Note I of the Supplemental Material [45]) and it is unreasonable that the device temperature would reach such high values for the low injection current used (150 mA/cm^2), under active cooling conditions. On the other hand, at 296 K, reciprocity analysis works fairly well for TAPC:C_{60} without the assumption of elevated device temperature, which is expected for a device that operates very close to quasi-thermal equilibrium at room temperature according to our prediction in Fig. 5. This further strengthens our hypothesis regarding non-thermal occupation of carriers being responsible for the EL peak mismatch for the blends discussed in Fig. 5.

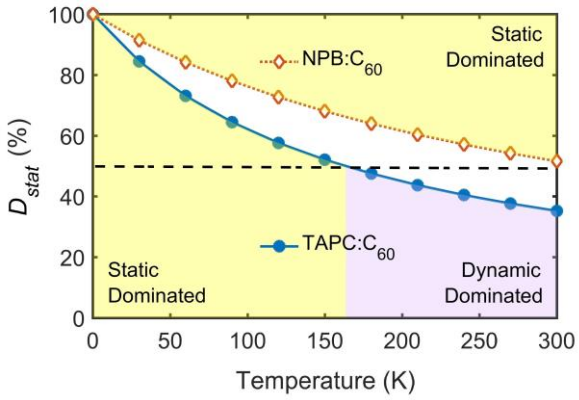

Figure 6. Relative contribution of the static disorder broadening (D_{stat}) in the total CT absorption spectral linewidth for TAPC:C_{60} (blue circles) and NPB:C_{60} (red diamonds). The linewidth is static disorder dominated below ~165 and ~300 K, respectively for TAPC and NPB devices.

From the discussion above, it is apparent that the complete CT DOS is represented in the CT absorption spectra, whereas the EL spectra in some cases fail to provide such representation owing to a non-thermal distribution of carriers. Once the CT energetic distribution (σ_{CT}) is extracted from temperature dependent EQE measurements (Fig. 3), one could determine the relative contribution of the static disorder in the CT state DOS using the parameters extracted from the absorption measurements, following, $D_{stat} = \frac{\sigma_{CT}^2}{\sigma_{CT}^2 + 2k_B\lambda T} \times 100\%$, originally described for the EL spectral linewidth [16]. For TAPC:C_{60} devices at room temperature D_{stat} is ~35%, which increases as the temperature lowers, eventually dominating the spectra below ~165 K (Fig. 6). For NPB:C_{60}, even at room temperature, static disorder dominates over the dynamic disorder contribution to the total spectral linewidth (Fig. 6). Although the D_{stat} values are estimated from the absorption spectra, these should be relevant for the emission spectra as well, if the injected carriers are close to thermal equilibrium and the reciprocity relation is applicable (TAPC:C_{60} at RT for example). However, higher D_{stat} might not automatically mean that the devices are operating out of thermal equilibrium. Thermal-equilibrium operation of the device, meaning whether the carriers would reach the sites associated to the lowest energy states in the DOS, would depend on the morphology induced variation in the CT energy, i.e., the relative values of the σ_{CT} of the D-A blends, rather than the D_{stat}.

4. Outlook and Conclusion

Discussion of energetic disorder and its effect on the spectral properties of OPVs have gained significant attention recently [12,13,16,51]. At the same time, whether the carriers in an OPV operate are at equilibrium, an effect most relevant for highly disordered blends, remains an open question [13,40]. Non-equilibrium operation of the solar cells could potentially redefine the thermodynamic performance limit and the way the OPV absorption-emission spectra are interpreted. In this work, we have demonstrated that CT state absorption and emission spectral shape and peaks are in fact influenced by the energetic disorder in the D-A blend, studying two archetypal small molecule organic solar cells, TAPC:C_{60} and NPB:C_{60}, with the latter having almost 1.5 times larger standard deviation (σ_{CT}) of the CT energetic distribution. We have shown that Burke et al.'s modification of the Marcus description of CT spectral function [10] through consideration of Gaussian energetic disorder, can effectively describe the low-energy subgap absorption spectra regardless of the degree of static disorder in the blend and the operating temperature. However, this approach can only explain the experimental emission spectra to the temperature value for which the injected carriers fully relax to the lowest energy CT state sites. For TAPC:C_{60}, this value is below room temperature and we can describe the emission spectra quite well with this formalism at the higher temperature range. On the other hand, for NPB:C_{60}, even the room temperature EL spectral peak is much higher than what is expected from fully relaxed charge carriers. In this case, the complete CT DOS, which is represented in the absorption spectra, might not be fully appreciated from the EL spectral shape and position. Hence it is ideal to estimate the relative contribution of the static and dynamic disorders in the CT spectral linewidth from the absorption data. Also, caution should be used when fitting the experimental emission spectra to extract E_{CT} and linewidth, since the representative equations (Eq. 2 and 4) are derived from the CT absorption spectra under the assumption of quasi-thermal equilibrium population of CT excitons. The value of the CT energetic disorder (σ_{CT}), which is linked to the ability of injected carriers being able to reach the lowest possible energy sites, influences the emission peak position and linewidth. Thus, proper estimation of σ_{CT} is important, for which temperature dependent CT absorption or EQE measurements are critical. It is worth noting two cases where this method of estimating static disorder in the blend is complicated: (1) heterojunction solar cells with large frontier orbital offsets [52], where EQE might not represent the CT DOS tail, and (2) solar cells where the CT state has strong overlap with the local exciton, where the resultant EQE spectra have no visible CT shoulder to fit a Gaussian function. Regardless of these exceptions, estimation of the average energetic disorder in the D-A blend should be applicable for most OPVs, and is a useful method to visualize the full extent of the low energy CT states that are otherwise invisible from emission measurements, but participate in fundamental photophysical processes like carrier generation, transport, and recombination and could aid in evaluating the influence of static disorder on energy loss.

Acknowledgments

This work was supported by the U.S. Department of Energy, Office of Basic Energy Sciences under Award No. DE-SC0012458.

References

[1] Y. Cui, H. Yao, J. Zhang, K. Xian, T. Zhang, L. Hong, Y. Wang, Y. Xu, K. Ma, C. An, C. He, Z. Wei, F. Gao, and J. Hou, Single- Junction Organic Photovoltaic Cells with Approaching 18% Efficiency, Adv. Mater. **32**, 1908205 (2020).

[2] M. A. Green, E. D. Dunlop, J. Hohl- Ebinger, M. Yoshita, N. Kopidakis, and A. W. Y. Ho- Baillie, Solar Cell Efficiency Tables (Version 55), Prog. Photovoltaics Res. Appl. **28**, 3 (2020).

[3] N. C. Giebink, G. P. Wiederrecht, M. R. Wasielewski, and S. R. Forrest, Thermodynamic Efficiency Limit of Excitonic Solar Cells, Phys. Rev. B **83**, 195326 (2011).

[4] K. Vandewal, K. Tvingstedt, A. Gadisa, O. Inganäs, and J. V. Manca, On the Origin of the Open-Circuit Voltage of Polymer–Fullerene Solar Cells, Nat. Mater. **8**, 904 (2009).

[5] K. Vandewal, K. Tvingstedt, A. Gadisa, O. Inganäs, and J. V. Manca, Relating the Open-Circuit Voltage to Interface Molecular Properties of Donor:Acceptor Bulk Heterojunction Solar Cells, Phys. Rev. B **81**, 125204 (2010).

[6] S. M. Menke, N. A. Ran, G. C. Bazan, and R. H. Friend, Understanding Energy Loss in Organic Solar Cells: Toward a New Efficiency Regime, Joule **2**, 25 (2018).

[7] M. Azzouzi, J. Yan, T. Kirchartz, K. Liu, J. Wang, H. Wu, and J. Nelson, Nonradiative Energy Losses in Bulk-Heterojunction Organic Photovoltaics, Phys. Rev. X **8**, 031055 (2018).

[8] F. Gao and O. Inganäs, Charge Generation in Polymer–Fullerene Bulk-Heterojunction Solar Cells, Phys. Chem. Chem. Phys. **16**, 20291 (2014).

[9] K. Vandewal, J. Widmer, T. Heumueller, C. J. Brabec, M. D. McGehee, K. Leo, M. Riede, and A. Salleo, Increased Open-Circuit Voltage of Organic Solar Cells by Reduced Donor-Acceptor Interface Area, Adv. Mater. **26**, 3839 (2014).

[10] T. M. Burke, S. Sweetnam, K. Vandewal, and M. D. McGehee, Beyond Langevin Recombination: How Equilibrium Between Free Carriers and Charge Transfer States Determines the Open-Circuit Voltage of Organic Solar Cells, Adv. Energy Mater. **5**, 1500123 (2015).

[11] N. Zarrabi, O. J. Sandberg, S. Zeiske, W. Li, D. B. Riley, P. Meredith, and A. Armin, Charge-Generating Mid-Gap Trap States Define the Thermodynamic Limit of Organic

Photovoltaic Devices, Nat. Commun. **11**, 5567 (2020).

[12] F. J. Kahle, A. Rudnick, H. Bässler, and A. Köhler, How to Interpret Absorption and Fluorescence Spectra of Charge Transfer States in an Organic Solar Cell, Mater. Horizons **5**, 837 (2018).

[13] A. Melianas, N. Felekidis, Y. Puttisong, S. C. J. Meskers, O. Inganäs, W. M. Chen, and M. Kemerink, Nonequilibrium Site Distribution Governs Charge-Transfer Electroluminescence at Disordered Organic Heterointerfaces, Proc. Natl. Acad. Sci. U. S. A. **116**, 23416 (2019).

[14] W. Gong, M. A. Faist, N. J. Ekins-Daukes, Z. Xu, D. D. C. Bradley, J. Nelson, and T. Kirchartz, Influence of Energetic Disorder on Electroluminescence Emission in Polymer: Fullerene Solar Cells, Phys. Rev. B - Condens. Matter Mater. Phys. **86**, 024201 (2012).

[15] R. C. I. MacKenzie, T. Kirchartz, G. F. A. Dibb, and J. Nelson, Modeling Nongeminate Recombination in P3HT:PCBM Solar Cells, J. Phys. Chem. C **115**, 9806 (2011).

[16] T. Linderl, T. Zechel, A. Hofmann, T. Sato, K. Shimizu, H. Ishii, and W. Brütting, Crystalline versus Amorphous Donor-Acceptor Blends: Influence of Layer Morphology on the Charge-Transfer Density of States, Phys. Rev. Appl. **13**, 024061 (2020).

[17] C. Kästner, K. Vandewal, D. A. M. Egbe, and H. Hoppe, Revelation of Interfacial Energetics in Organic Multiheterojunctions, Adv. Sci. **4**, 1600331 (2017).

[18] U. Albrecht and H. Bässler, Yield of Geminate Pair Dissociation in an Energetically Random Hopping System, Chem. Phys. Lett. **235**, 389 (1995).

[19] T. M. Burke and M. D. McGehee, How High Local Charge Carrier Mobility and an Energy Cascade in a Three-Phase Bulk Heterojunction Enable >90% Quantum Efficiency, Adv. Mater. **26**, 1923 (2014).

[20] T. Offermans, S. C. J. Meskers, and R. A. J. Janssen, Charge Recombination in a Poly(Para-Phenylene Vinylene)-Fullerene Derivative Composite Film Studied by Transient, Nonresonant, Hole-Burning Spectroscopy, J. Chem. Phys. **119**, 10924 (2003).

[21] R. A. Street, Localized State Distribution and Its Effect on Recombination in Organic Solar Cells, Phys. Rev. B **84**, 075208 (2011).

[22] T. Kirchartz, B. E. Pieters, J. Kirkpatrick, U. Rau, and J. Nelson, Recombination via Tail States in Polythiophene:Fullerene Solar Cells, Phys. Rev. B - Condens. Matter Mater. Phys. **83**, 115209 (2011).

[23] A. V. Nenashev, J. O. Oelerich, and S. D. Baranovskii, Theoretical Tools for the Description of Charge Transport in Disordered Organic Semiconductors, J. Phys. Condens. Matter **27**, 093201 (2015).

[24] J. Widmer, Charge Transport and Energy Levels in Organic Semiconductors Ph.D. thesis,

TU Dresden (2019).

[25] N. C. Giebink, B. E. Lassiter, G. P. Wiederrecht, M. R. Wasielewski, and S. R. Forrest, Ideal Diode Equation for Organic Heterojunctions. II. the Role of Polaron Pair Recombination, Phys. Rev. B - Condens. Matter Mater. Phys. **82**, 155306 (2010).

[26] R. A. Street, K. W. Song, J. E. Northrup, and S. Cowan, Photoconductivity Measurements of the Electronic Structure of Organic Solar Cells, Phys. Rev. B - Condens. Matter Mater. Phys. **83**, 165207 (2011).

[27] J. C. Blakesley and D. Neher, Relationship between Energetic Disorder and Open-Circuit Voltage in Bulk Heterojunction Organic Solar Cells, Phys. Rev. B - Condens. Matter Mater. Phys. **84**, 075210 (2011).

[28] K. Tvingstedt, J. Benduhn, and K. Vandewal, Temperature Dependence of the Spectral Line-Width of Charge-Transfer State Emission in Organic Solar Cells; Static vs. Dynamic Disorder , Mater. Horizons **7**, 1888 (2020).

[29] A. N. Brigeman, M. A. Fusella, Y. Yan, G. E. Purdum, Y.-L. Loo, B. P. Rand, and N. C. Giebink, Revealing the Full Charge Transfer State Absorption Spectrum of Organic Solar Cells, Adv. Energy Mater. **6**, 1601001 (2016).

[30] L. Goris, K. Haenen, M. Nesládek, P. Wagner, D. Vanderzande, L. De Schepper, J. D'haen, L. Luisen, and J. V. Manca, Absorption Phenomena in Organic Thin Films for Solar Cell Applications Investigated by Photothermal Deflection Spectroscopy, in Journal of Materials Science **40**, 1413 (2005).

[31] M. C. Scharber, C. Lungenschmied, H. J. Egelhaaf, G. Matt, M. Bednorz, T. Fromherz, J. Gao, D. Jarzab, and M. A. Loi, Charge Transfer Excitons in Low Band Gap Polymer Based Solar Cells and the Role of Processing Additives, Energy Environ. Sci. **4**, 5077 (2011).

[32] R. A. Marcus, Relation between Charge Transfer Absorption and Fluorescence Spectra and the Inverted Region, J. Phys. Chem. **93**, 3078 (1989).

[33] U. Rau, Reciprocity Relation between Photovoltaic Quantum Efficiency and Electroluminescent Emission of Solar Cells, Phys. Rev. B **76**, 085303 (2007).

[34] K. Vandewal, J. Benduhn, K. S. Schellhammer, T. Vangerven, J. E. Rückert, F. Piersimoni, R. Scholz, O. Zeika, Y. Fan, S. Barlow, D. Neher, S. R. Marder, J. Manca, D. Spoltore, G. Cuniberti, and F. Ortmann, Absorption Tails of Donor:C 60 Blends Provide Insight into Thermally Activated Charge-Transfer Processes and Polaron Relaxation, J. Am. Chem. Soc. **139**, 1699 (2017).

[35] S. Ullbrich, J. Benduhn, X. Jia, V. C. Nikolis, K. Tvingstedt, F. Piersimoni, S. Roland, Y. Liu, J. Wu, A. Fischer, D. Neher, S. Reineke, D. Spoltore, and K. Vandewal, Emissive and Charge-Generating Donor–Acceptor Interfaces for Organic Optoelectronics with Low Voltage Losses, Nature Materials **18**, 459 (2019).

[36] Y. L. Lin, F. Zhang, R. A. Kerner, T. C.-J. Yang, A. Kahn, and B. P. Rand, Variable Charge Transfer State Energies at Nanostructured Pentacene/C 60 Interfaces, Appl. Phys. Lett. **112**, 213302 (2018).

[37] Y. L. Lin, M. A. Fusella, and B. P. Rand, The Impact of Local Morphology on Organic Donor/Acceptor Charge Transfer States, Adv. Energy Mater. **8**, 1702816 (2018).

[38] S. Roland, J. Kniepert, J. A. Love, V. Negi, F. Liu, P. Bobbert, A. Melianas, M. Kemerink, A. Hofacker, and D. Neher, Equilibrated Charge Carrier Populations Govern Steady-State Nongeminate Recombination in Disordered Organic Solar Cells, J. Phys. Chem. Lett. **10**, 1374 (2019).

[39] M. A. Fusella, A. N. Brigeman, M. Welborn, G. E. Purdum, Y. Yan, R. D. Schaller, Y. L. Lin, Y.-L. Loo, T. Van Voorhis, N. C. Giebink, and B. P. Rand, Band-like Charge Photogeneration at a Crystalline Organic Donor/Acceptor Interface, Adv. Energy Mater. **8**, 1701494 (2018).

[40] A. N. Brigeman, M. A. Fusella, B. P. Rand, and N. C. Giebink, Nonthermal Site Occupation at the Donor-Acceptor Interface of Organic Solar Cells, Phys. Rev. Appl. **10**, 034034 (2018).

[41] K. Tvingstedt, K. Vandewal, A. Gadisa, F. Zhang, J. Manca, and O. Inganäs, Electroluminescence from Charge Transfer States in Polymer Solar Cells, J. Am. Chem. Soc. **131**, 11819 (2009).

[42] K. Tvingstedt, K. Vandewal, F. Zhang, and O. Inganäs, On the Dissociation Efficiency of Charge Transfer Excitons and Frenkel Excitons in Organic Solar Cells: A Luminescence Quenching Study, J. Phys. Chem. C (2010).

[43] C. Kulshreshtha, J. W. Choi, J. Kim, W. S. Jeon, M. C. Suh, Y. Park, and J. H. Kwon, Open-Circuit Voltage Dependency on Hole-Extraction Layers in Planar Heterojunction Organic Solar Cells, Appl. Phys. Lett. **99**, 023308 (2011).

[44] M. Li, W. Zhang, H. Wang, L. Chen, C. Zheng, and R. Chen, Effect of Organic Cathode Interfacial Layers on Efficiency and Stability Improvement of Polymer Solar Cells, RSC Adv. **7**, 31158 (2017).

[45] See Supplemental Material at [URL Will Be Inserted by Publisher] for molecular structures, CT EQE fitting details, complete EL spectral data, EL-EQE reciprocity analysis, and note on low temperature measurements.

[46] F. Gao, W. Tress, J. Wang, and O. Inganäs, Temperature Dependence of Charge Carrier Generation in Organic Photovoltaics, Phys. Rev. Lett. **114**, 128701 (2015).

[47] D. Spoltore, A. Hofacker, J. Benduhn, S. Ullbrich, M. Nyman, O. Zeika, S. Schellhammer, Y. Fan, I. Ramirez, S. Barlow, M. Riede, S. R. Marder, F. Ortmann, and K. Vandewal, Hole Transport in Low-Donor-Content Organic Solar Cells, J. Phys. Chem. Lett. **9**, 5496 (2018).

[48] T. Kirchartz, J. Nelson, and U. Rau, Reciprocity between Charge Injection and Extraction and Its Influence on the Interpretation of Electroluminescence Spectra in Organic Solar Cells, Phys. Rev. Appl. **5**, 054003 (2016).

[49] W. Boukhili, M. Mahdouani, R. Bourguiga, and J. Puigdollers, Characterization and Modeling of Organic Thin-Film Transistors Based π-Conjugated Small Molecule Tetraphenyldibenzoperiflanthene: Effects of Channel Length, Microelectron. Eng. **160**, 39 (2016).

[50] B. P. Rand, J. Xue, S. Uchida, and S. R. Forrest, Mixed Donor-Acceptor Molecular Heterojunctions for Photovoltaic Applications. I. Material Properties, J. Appl. Phys. **98**, 124902 (2005).

[51] C. Göhler, M. Saladina, Y. Wang, D. Spoltore, J. Benduhn, K. Leo, and C. Deibel, Temperature-Dependent Charge-Transfer-State Absorption and Emission Reveal the Dominant Role of Dynamic Disorder in Organic Solar Cells, Phys. Rev. Appl. **15**, 064009 (2021).

[52] S.-U.-Z. Khan, G. Londi, X. Liu, M. A. Fusella, G. D'Avino, L. Muccioli, A. N. Brigeman, B. Niesen, T. C.-J. Yang, Y. Olivier, J. T. Dull, N. C. Giebink, D. Beljonne, and B. P. Rand, Multiple Charge Transfer States in Donor–Acceptor Heterojunctions with Large Frontier Orbital Energy Offsets, Chem. Mater. **31**, 6808 (2019).